# Equatorially confined warm trapped ions at around 100 eV near the plasmapause

Masatoshi Yamauchi, Iannis Dandouras, Henri Rème, Farida El-Lemdani Mazouz

# Equatorially confined warm trapped ions at around 100 eV near the plasmapause

M. Yamauchi,[1] I. Dandouras,[2,3] H. Rème,[2,3] and F. El-Lemdani Mazouz[4]

Received 12 May 2012; revised 21 June 2012; accepted 21 June 2012; published 1 August 2012.

[1] Near the equatorial plasmapause at around 4–5 Earth radius ($R_E$) geocentric distance, pancake distributed tens of eV ions are sometimes found, as previously reported by Olsen et al. (1987). Cluster CIS data during perigee traversals in 2001–2002 (nearly 200 traversals) revealed new features of these equatorially-trapped warm ions. (1) The characteristic energy of $He^+$ is often higher than that of $H^+$. (2) Some events show non-thermal ring distribution for $He^+$ rather than superthermal pancake distribution. $H^+$ can also have the ring distribution in such events. (3) While majority of the events are dispersion-free, some events show energy-time dispersion, indicating drifts from different local times. (4) The time scale of the development is about an hour, which is much shorter than the drifting time of these ions around the Earth. Cluster statistics also confirmed some results from the previous studies: (5) These ions are confined within a few degrees of latitudinal range near the equator, and have nearly 90° pitch angles. (6) At a geocentric distance of about 4–4.5 $R_E$ where Cluster traversed the equator during its perigee, the probability of observing clear events is about 40–45% in the noon and dusk sectors and about 20–25% in the night-to-dawn sector. (7) They are dominated by $H^+$ with variable content of $He^+$. The $He^+/H^+$ ratio is much less than 5% for the majority of the cases. **Citation:** Yamauchi, M., I. Dandouras, H. Rème, and F. El-Lemdani Mazouz (2012), Equatorially confined warm trapped ions at around 100 eV near the plasmapause, *Geophys. Res. Lett.*, *39*, L15101, doi:10.1029/2012GL052366.

## 1. Introduction

[2] Near the plasmapause, localized enhancement of low-energy ion flux is often observed. Its form can be either density enhancement [*Chappell et al.*, 1971] or temperature enhancement [*Olsen*, 1981]. The density enhancement (cold dense plume of plasmaspheric origin) has long been studied, and some types (i.e., cloaks) are known to detach and drain [e.g., *Borovsky and Denton*, 2008; *Darrouzet et al.*, 2009, and references therein]. The temperature enhancement has not been studied very much for more than two decades after *Olsen et al.* [1987] demonstrated the morphology of warm trapped ions within a few degree latitudinal range near the equator using low-energy ion instruments that cover up to 50 eV [see also *Lennartsson and Reasoner*, 1978; *Olsen*, 1981; *Olsen et al.*, 1994]. These warm ions show a pancake distribution (nearly 90° pitch angles) with the perpendicular temperature of tens of eV [*Olsen et al.*, 1987]. We call these ions "equatorially-trapped warm ions" hereafter.

[3] The other results from *Olsen et al.* [1987] are summarized as follows. The equatorially-trapped warm ions are primarily composed of $H^+$. The plasma density obtained from the wave instrument is nearly unchanged between inside and outside the equatorially-trapped warm ions; i.e., the observed flux enhancement is mainly due to the temperature increase. The $He^+/H^+$ ratio of these warm ions is normally much less than 5%, although some cases show about the same $He^+/H^+$ ratio as the cold plasmaspheric component, i.e., 5∼10%. When $He^+$ are detected, they have about the same temperature as $H^+$. These observations led Olsen et al. to conclude that at least heavy ions are not preferentially heated compared to $H^+$. Thus, this is a different phenomenon from the cold plasmaspheric plume [e.g., *Darrouzet et al.*, 2008].

[4] The equatorially-trapped warm ions are observed during nearly all geomagnetic conditions, and are mainly found at 3∼5 $R_E$ at all local times (4∼5 $R_E$ in the dusk side and <4 $R_E$ in the dawn side) except 4∼8 MLT where they can be distributed at <3 $R_E$ where DE-1 satellite did not traverse [*Olsen et al.*, 1987]. The pancake-distributed tens of eV ions are also found by low-inclination satellites such as geosynchronous satellites [*Horwitz et al.*, 1981], in which the pitch angle distribution is consistent with the confinement to the equator [*Olsen et al.*, 1994].

[5] During the perigee traversals, the Cluster satellites crossed nearly perpendicular to the equatorial plane at 4–5 $R_E$ geocentric distance. Cluster Ion Spectrometry (CIS) [*Rème et al.*, 2001] measures ions at the relevant and wide energy range (0.03–40 keV for COmposition DIstribution Function (CODIF) with mass separation and 0.005–40 keV for Hot Ion Analyser (HIA) without mass separation), and has sufficient sensitivity to reveal the characteristics of the equatorially-trapped warm ions. Therefore, Cluster is an ideal mission to study these ions, and we actually found new features with CIS, which we report in this paper. We primarily use the CODIF data because it is much less contaminated by the radiation belt particles than HIA. The general CIS observations during Cluster perigee traversals are summarized in *Darrouzet et al.* [2009] *and Dandouras et al.* [2009]. Unfortunately, the electron data at the relevant

[1]Swedish Institute of Space Physics, Kiruna, Sweden.
[2]Institut de Recherche en Astrophysique et Planétologie, UPS-OMP, University of Toulouse, Toulouse, France.
[3]Institut de Recherche en Astrophysique et Planétologie, CNRS, Toulouse, France.
[4]Laboratoire Atmosphère, Milieux, Observation Spatiales, Guyancourt, France.

Corresponding author: M. Yamauchi, Swedish Institute of Space Physics, Box 812, Kiruna SE-98128, Sweden. (m.yamauchi@irf.se)


0094-8276/12/2012GL052366

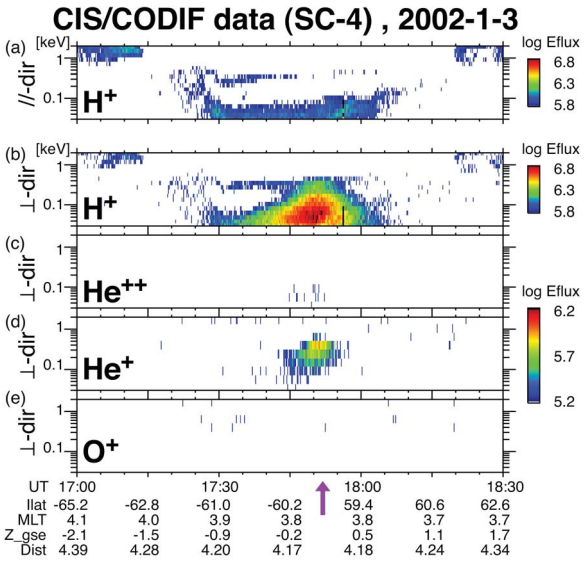


**Figure 1.** Energy-time spectrograms of differential energy flux (keV $cm^{-2}$ $s^{-1}str^{-1}$ $keV^{-1}$) observed by CIS/CODIF on board Cluster SC-4 during perigee traversal on 3 January 2002 during 17:00∼18:30 UT. Since the spacecraft spin is nearly along the geomagnetic field near the equatorial plane, eight different looking directions of the instrument correspond to nearly constant pitch angles (with about ±20° fluctuation): direction = 1 nearly anti-parallel to the geomagnetic field from north to south, and direction = 8 nearly parallel to the geomagnetic field from south to north. (a) Average of looking directions 1, 2, 7, and 8, i.e., parallel and anti-parallel directions to the geomagnetic field covering up to 45° pitch angles. (b–e) Average of directions 4 and 5, i.e., nearly perpendicular direction to the geomagnetic field. Ion species are indicated in each panel. The vertical arrow at the bottom indicates the crossing of the equatorial plane that is identified by the wave activity observed by WHISPER.

energy range are not available due to heavy contamination by the radiation belt particles.

## 2. Observations

[6] Figure 1 shows an example of the equatorially-trapped warm ions. The data are taken from the perigee traversal near the equator. The geomagnetic activity was quiet for 18 h except for a period of minor activity (AL = −150 nT) at 6∼9 h before this event. In Figure 1, the looking direction within the equator, i.e., the perpendicular direction to the geomagnetic field, is presented for four species ($H^+$, $He^{++}$, $He^+$, and $O^+$), while the field-aligned direction (looking north and south within about a 45° cone angle) is presented only for $H^+$.

[7] At around 17:50 UT, an intense $H^+$ signature at around 40∼200 eV is recognized together with a clear $He^+$ signature at higher energy than $H^+$. It is observed very close to the equator that is identified by the wave activity observed by WHISPER (e.g., the $(n + 0.5)f_{ce}$ burst, where $f_{ce}$ is the electron cyclotron frequency, and $n \geq 1$ [*El-Lemdani Mazouz et al.*, 2009, and references therein]). Neither $He^{++}$ nor $O^+$ signature is recognized in the spectrogram (the faint count of $He^{++}$ is contamination of $H^+$). The signature is seen only in the perpendicular direction to the geomagnetic field, but not in the parallel or anti-parallel direction to the geomagnetic field up to at least 45° pitch angles. These ions are the equatorially-trapped warm ions.

[8] We examined all perigee traversals during 2001–2002 when the sensitivity of the instrument was highest before degradation of the sensor by the radiation belt dose became significant for this specific phenomenon after 2003. During this period, CODIF was operated much more frequently on SC-4 than on SC-1 or SC-3 (it did not work on SC-2). Therefore, we use SC-4 for statistics. There are a total of 187 traversals with CODIF observations by SC-4, in which 23 traversals are highly contaminated by the radiation belt particles and are removed. The remaining 164 traversals are examined.

[9] Out of these 164 traversals, the equatorially-trapped warm ions are clearly identified in 56 traversals while we could not find any signature in 85 traversals. The remaining 23 traversals are unclear. Thus, the probability of observing the equatorially-trapped warm ions by a single spacecraft is about 35–45%. The observation probability is increased by about 5% if we count all traversals when one of the three spacecraft detected the event because in some cases only one or two spacecraft detected them. This 5% difference most likely reflects the time scale of the phenomenon, as discussed later. Note that CODIF does not measure ions with energy <30 eV during the normal mode, and therefore, the occurrence probability of all events may even be higher.

[10] We also examined the local time distribution. Since the statistics are not very large, we divided the data into only four sectors, dawn, noon, dusk, and night. Figure 2 summarizes the probability of observing the equatorially-trapped warm ions by SC-4 at each sector. The probability is higher in the noon and dusk sectors (nearly half the traversals) than in the night-to-dawn sector (about one quarter of the traversals). The probabilities of observing the event by one of three spacecraft are again about 5–10% higher than

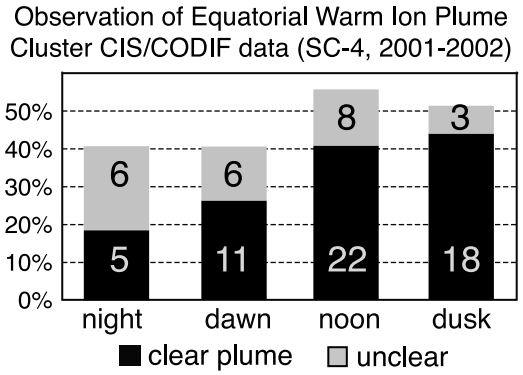


**Figure 2.** Probabilities of observing the equatorially-trapped warm ions by CIS/CODIF on SC-4 at different sectors during 2001–2002. Since Cluster orbit is synchronous to the solar system, sectors are defined as dusk when Cluster traversed the equator during 16 April–15 July, noon during 16 July–15 October, dawn during 16 October–15 January, and night during 16 January–15 April. The unclear cases mean the observations that we could not judge, i.e., belong to the error range. The number in each bar represents the number of traversals.

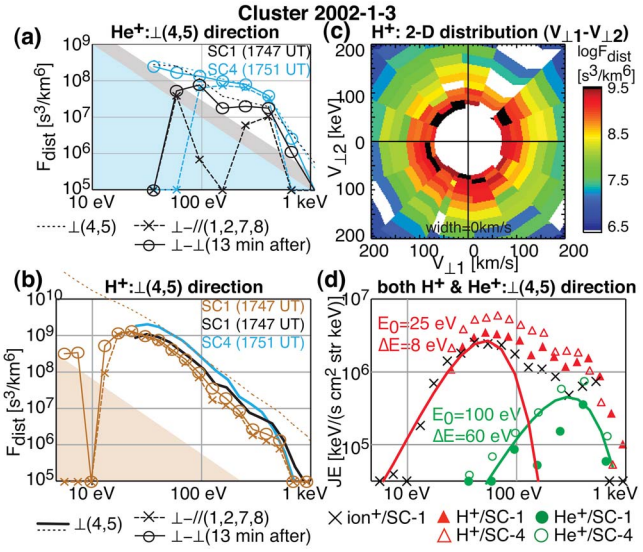


**Figure 3.** Average distribution functions ($f_\perp$) in the perpendicular direction to the magnetic field ($\perp$) over 7–8 spins (about 1∼2 min) for (a) $He^+$ (CODIF), and (b) $H^+$ (CODIF) and total ions (HIA: brown), obtained from SC-1 (black and brown) and SC-4 (blue). HIA and CODIF $H^+$ channels have the same energy bins in these plots, and one-count levels are shown by the hatched areas with the same colors as the plots. To subtract the contamination background by the radiation belt particles for $He^+$ and total ions ($H^+$ does not need subtraction), we tried two methods: (1) by subtracting the distribution function in the field-aligned direction (//), as denoted by crosses; (2) by subtracting $f_\perp$ at the time without the warm ion signature (13 min after the event), as denoted by circles. Unfortunately, neither method can fully subtracts the background, and therefore, the actual $f_\perp$ is most likely below the circles and crosses. (c) Velocity-space distribution function of $H^+$ for energy <2 keV observed by SC-4 (CODIF). A 2-D cut in the $\perp$ perpendicular plane is displayed for one spin starting at 1751:00 UT. The circler white void region corresponds to $H^+ < 25$ eV, for which CODIF does not measure. (d) Energy flux for $H^+$ (red triangles), $He^+$ (green circles), and total ions (crosses). The radiation belt contamination is subtracted by the second method. One-count levels are below the horizontal axis ($3\cdot10^4$ cm$^{-2}$ s$^{-1}$str$^{-1}$). The solid lines are Gaussian fittings $f_\perp \propto E^2\cdot\exp[(\sqrt{E} - \sqrt{E_0})^2/\Delta E]$ for $H^+$ (red) and $He^+$ (green), respectively.

these values. The drop of the probability in the night-to-dawn sector agrees with the cold ion (<50 eV) measurements by DE-1 [*Olsen et al.*, 1987, plate 7], in which the equatorially-trapped warm ions are observed at a shorter geocentric distance (<4 $R_E$) in the night-to-dawn sector than in the other sectors.

[11] One new feature that Cluster revealed is the energy distribution beyond 50 eV. Figures 3a and 3b show the 1-D distribution function in the perpendicular direction to the geomagnetic field ($f_\perp$) for $He^+$ and $H^+$, respectively. We overlaid the observation by SC-1 that crossed the equator about 3 min before SC-4. Since data from HIA and CODIF $He^+$ channel are highly contaminated by the radiation belt particles, we tried to reduce the contamination by two methods (see figure caption). After such corrections, the HIA (total ion) data agrees with the CODIF $H^+$ data for both spacecraft, confirming the decreasing trend toward zero energy. This trend is more obvious for $He^+$. Thus, the distribution functions for $H^+$ and particularly $He^+$ have peaks at non-zero energies. These offsets are not due to convection because typical drift velocity of 1 LT/h at 4 $R_E$ corresponds to about 2 km/s (0.1 eV) and is below the instrumental limit. In fact, the distribution is nearly gyrotropic according to a 2-D distribution perpendicular to the magnetic field as shown in Figure 3c. A gyrotropic distribution with peak at non-zero energy means a ring distribution. A Gaussian fitting of $\propto E^2\cdot\exp[(\sqrt{E} - \sqrt{E_0})^2/\Delta E]$ to the energy flux as shown in Figure 3d yields the center energies ($E_0$) for the $He^+$ and $H^+$ rings of 100 eV and 25 eV, respectively, for this example. The fitting of $H^+$ is not perfect for high-energy part, indicating more effective energization for higher energy.

[12] By choosing traversals during 2001–2002 in which the $He^+$ channel is not contaminated very much by the radiation belt electrons, we found 29 intense events that have peak differential energy fluxes for $H^+$ of more than $3\cdot10^6$ keV cm$^{-2}$ s$^{-1}$str$^{-1}$ keV$^{-1}$. Note that this threshold might be overestimated, because the count rate increases drastically for the same flux when contamination by the radiation belt particles increases, and because the effect of the radiation belt is not zero in this region. Out of these 29 examples, 10 cases showed identifiable $He^+$ at clearly higher energy than $H^+$; 13 cases are without $He^+$ signature; 3 cases showed minor $He^+$ signature at the same energy as $H^+$ but the intensity is so low that we could not discern the signature from $H^+$ contamination; and 3 cases showed clear $He^+$ signature at the same energy as $H^+$. The ratio of the characteristic energies (energies of peak energy flux) between $He^+$ and $H^+$ varies in different examples. In addition, three more cases showed only $He^+$ near 30 eV (lower energy threshold) such that the absence of the $H^+$ count may well be interpreted as the energization of $H^+$ being less than 30 eV.

[13] Except for the energy distribution of $He^+$ and $H^+$, we have the same result as *Olsen et al.* [1987]: the coexistence of the $He^+$ with the equatorially-trapped warm protons is quite variable and the $He^+/H^+$ ratio is much less than 5% in most cases. We also searched an $O^+$ signature in these 29 cases because *Olsen et al.* [1987] found one case with $O^+$. However, we could not identify clear $O^+$ signatures beyond the background level, partly because the contamination by the radiation belt particles is severer in $O^+$ data than in $He^+$ data. On the other hand, we found two cases with clear $O^+$ signature at higher energy than $He^+$ when only $He^+$ is observed near 30 eV without $H^+$. Both cases are observed during the recovery phase of magnetic storms.

[14] With multi-spacecraft, Cluster also revealed temporal development of the equatorially-trapped warm ions. Figure 4 shows CODIF data from three spacecraft. All the spacecraft crossed the magnetic equator at nearly the same local time (16.8 MLT) at slightly different UT and geocentric distances: SC-1 at around 04:48 UT (4.3 $R_E$), SC-4 at around 04:50 UT (4.0 $R_E$), and SC-3 at around 05:31 UT (4.2 $R_E$). The absence of the warm ion signature in SC-1 and -4 indicates the absence at 4.0∼4.3 $R_E$ geocentric distances at around 04:50 UT. Therefore, the clear signature of the equatorially-trapped warm ions observed 40 min later by SC-3 means a sudden appearance of the warm ions within 40 min. This time scale is much shorter than the time scale of ion drift around the Earth at this energy. The short time scale partly

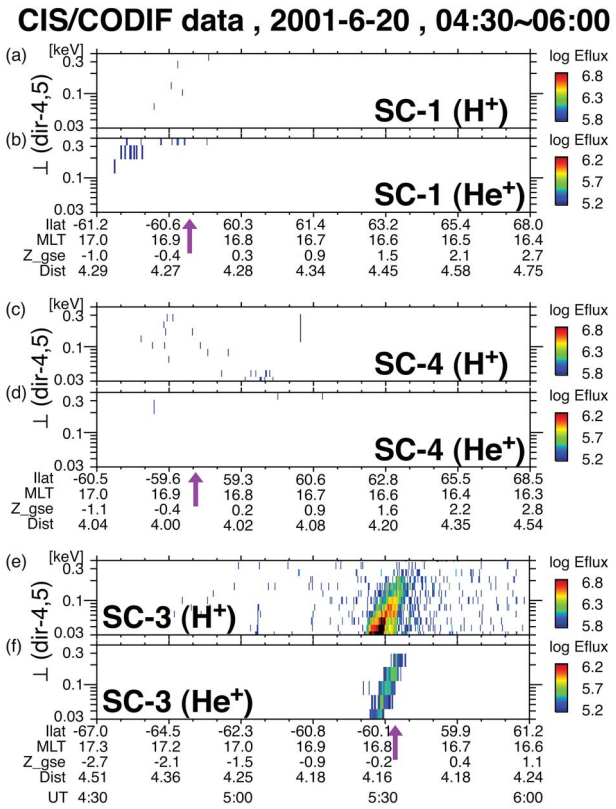


**Figure 4.** Cluster ion (CIS/CODIF) data from SC-1, 3, and 4 during perigee traversal on 20 June, 2001 during 4:30∼6:00 UT. The format is similar to Figure 1, showing $H^+$ and $He^+$ data in the perpendicular directions to the geomagnetic field for (a and b) SC-1, (c and d) SC-4, and (e and f) SC-3.

explains the different probabilities of the detection between single spacecraft and one of three spacecraft and between different sectors. We examined all traversals during 2001–2002 with a spacecraft separation of more than 40 min, and found that the majority of them showed substantial changes in the intensity (by more than factor of 5).

[15] The last new feature of the equatorially-trapped warm ions is energy-time dispersion, which is recognized in Figure 4. Out of 29 intense $H^+$ events identified by SC-4, five cases showed clear energy-time dispersion, and all dispersions show energy increasing with time. Since it is exactly at the equator and perigee, this dispersion cannot come from a spatial structure, and must come from different time-of-flight of ion drifts at different energies. The strength of the dispersion can be used to estimate the source distance and time-of-flight.

[16] The energy-independent E × B drift (including corotation) determines the main motion of low energy ions, and the energy-dependent magnetic drift ($V_B$[MLT/h] ∼ 0.35 W[keV] at around 4 $R_E$) causes the energy-time dispersion, where W is the energy of the equatorially-trapped ions [*Yamauchi et al.*, 2006]. For 150 eV ions and 30 eV ions, the magnetic drifts are about 0.05 MLT/h and about 0.01 MLT/h, respectively, causing a difference of 0.04 MLT/h. Since the E × B drift at 17 MLT is slightly slower than the co-rotation (1 MLT/h eastward), it takes about 3 min to drift over a distance of 0.04 MLT. This is the same as the observed time lag between the 30 eV and 150 eV signatures. Inversely, the dispersion in Figure 4e means that ions are heated about 1 h before at a limited MLT range (otherwise, we cannot explain the lower energy cut-off) at around 16 MLT. Such a new arrival scenario agrees with the absence of equatorially-trapped warm ions 40 min before.

## 3. Discussion

[17] Many questions remained for future study. One is the cause of different characteristic energies between $H^+$ and $He^+$, and of the ring distribution in some cases. The ring distribution indicates non-thermal heating such as resonance with waves. One possible scenario is multiple heating. Since the equatorial plasmapause is a region with many waves, it is possible that two heating mechanisms coexist: one pre-heating mechanism to the same temperature between $H^+$ and $He^+$, and the other post-heating mechanism to different energies. To answer this, we need a systematic examination between ion data and the wave data.

[18] The variable $He^+$ (and $O^+$) content is another mystery. We have not yet identified any special conditions for traversals with high $He^+$ content with CIS data. The last question is the source extent. The example in Figure 4 indicates a very narrow source region with temporal heating. On the other hand, dispersion-free cases (the majority) mean that the ions are energized very close to the spacecraft unless the energization is very uniform at a very extended source, which is unlikely. If the energization is local, the observation frequency of more than one third means that the energization takes place at many spots, and that should give a higher observation probability for dispersed cases than for non-dispersed cases. We have not yet found the answer to this discrepancy.

## 4. Conclusions

[19] Cluster CIS/CODIF observations during perigee traversals revealed new features of the equatorially-trapped warm ions.

[20] 1. The characteristic energy of $He^+$ is often higher than that of $H^+$.

[21] 2. Some events show a non-thermal ring distribution for $H^+$ and particularly for $He^+$ rather than superthermal pancake distribution.

[22] 3. While majority of the events are dispersion-free, some events show energy-time dispersion, indicating drifts from different local times.

[23] 4. The time scale of the development is about an hour, and is much shorter than the drifting time of these ions around the Earth.

[24] Cluster CIS data also confirmed some of the results of previous studies:

[25] 5. These ions are confined within a few degrees of latitudinal range near the equator, and have nearly 90° pitch angles.

[26] 6. At the geocentric distance of about 4–4.5 $R_E$ where Cluster traversed the equator at its perigee, the observation probability of clear events is about 40–45% in the noon and dusk sectors and about 20–25% in the night-to-dawn sector.

[27] 7. They are dominated by tens of eV $H^+$ with a variable content of $He^+$. The $He^+/H^+$ ratio is much less than 5% for the majority of the cases.

[28] We still have many questions left. Some may be solved by a thorough comparison between the ion data and wave data as well as by drift simulation. Some may be addressed in the coming Radiation Belt Storm Probes (RBSP) mission.

[29] **Acknowledgments.** The Cluster project is managed by ESA. The provisional AE index is provided by WDC-C2 for geomagnetism at Kyoto University. The Swedish part of the work is partly supported by the Swedish National Space Board (RS). We thank S. Grimald and J. Pickett for useful comments. The lead author (M.Y.) wishes to thank Sweden programs of providing help for physically disabled individuals, which have made it possible for him to conduct this work.

[30] The Editor thanks Scott Boardsen and an anonymous reviewer for their assistance in evaluating this paper.

## References

Borovsky, J. E., and M. H. Denton (2008), A statistical look at plasmaspheric drainage plumes, *J. Geophys. Res.*, *113*, A09221, doi:10.1029/2007JA012994.

Chappell, C. T., K. K. Harris, and G. W. Sharp (1971), The dayside of the plasmasphere, *J. Geophys. Res.*, *76*(31), 7632–7647, doi:10.1029/JA076i031p07632.

Dandouras, I., J. Cao, and C. Vallat (2009), Energetic ion dynamics of the inner magnetosphere revealed in coordinated Cluster–Double Star observations, *J. Geophys. Res.*, *114*, A01S90, doi:10.1029/2007JA012757.

Darrouzet, F., J. De Keyser, P. M. E. Décréau, F. El-Lemdani Mazouz, and X. Vallières (2008), Statistical analysis of plasmaspheric plumes with Cluster/WHISPER observation, *Ann. Geophys.*, *26*, 2403–2417, doi:10.5194/angeo-26-2403-2008.

Darrouzet, F., et al. (2009), Plasmaspheric density structures and dynamics: Properties observed by the CLUSTER and IMAGE missions, *Space Sci. Rev.*, *145*(1–2), 55–106, doi:10.1007/s11214-008-9438-9.

El-Lemdani Mazouz, F., J. L. Rauch, P. M. E. Décréau, J. G. Trotignon, X. Vallières, F. Darrouzet, P. Canu, and X. Suraud (2009), Wave emissions at half electron gyroharmonics in the equatorial plasmasphere region: CLUSTER observations and statistics, *Adv. Space Res.*, *43*, 253–264, doi:10.1016/j.asr.2008.06.007.

Horwitz, J. L., C. R. Baugher, C. R. Chappell, E. G. Shelley, and D. T. Young (1981), Pancake pitch angle distributions in warm ions observed with ISEE 1, *J. Geophys. Res.*, *86*(A5), 3311–3320, doi:10.1029/JA086iA05p03311.

Lennartsson, W., and D. L. Reasoner (1978), Low-energy plasma observations at synchronous orbit, *J. Geophys. Res.*, *83*(A5), 2145–2156, doi:10.1029/JA083iA05p02145.

Olsen, R. C. (1981), Equatorially trapped plasma populations, *J. Geophys. Res.*, *86*(A13), 11,235–11,245, doi:10.1029/JA086iA13p11235.

Olsen, R. C., S. D. Shawhan, D. L. Gallagher, J. L. Green, C. R. Chappell, and R. R. Anderson (1987), Plasma observations at the Earth's magnetic equator, *J. Geophys. Res.*, *92*(A3), 2385–2407, doi:10.1029/JA092iA03p02385.

Olsen, R. C., L. J. Scott, and S. A. Boardsen (1994), Comparison between Liouville's theorem and observed latitudinal distribution of trapped ions in the plasmapause region, *J. Geophys. Res.*, *99*(A2), 2191–2203, doi:10.1029/93JA02776.

Rème, H., et al. (2001), First multispacecraft ion measurements in and near the Earth's magnetosphere with the identical Cluster ion spectrometry (CIS) experiment, *Ann. Geophys.*, *19*(10–12), 1303–1354, doi:10.5194/angeo-19-1303-2001.

Yamauchi, M., et al. (2006), Source location of the wedge-like dispersed ring current in the morning sector during a substorm, *J. Geophys. Res.*, *111*, A11S09, doi:10.1029/2006JA011621.